Anharmonic motion and aspherical nuclear probability density functions in cesium halides

Thomas Bjørn Egede Grønbech,[1] Kasper Tolborg,[1] Davide Ceresoli,[2,*] and Bo Brummerstedt Iversen[1,†]
[1]*Center for Integrated Materials Research, Department of Chemistry, and iNANO, Aarhus University, Langelandsgade 140, DK-8000 Aarhus C, Denmark*
[2]*Istituto di Scienze e Tecnologie Chimiche "Giulio Natta" (SCITEC), National Research Council (CNR), I-20133, Milano, Italy*

(Received 5 January 2022; revised 1 March 2022; accepted 3 March 2022; published 29 March 2022)

The cesium halides (Cs*X*) are ionic high-symmetry compounds, which at first would seem like well-understood systems. However, recent studies have shown that using the simple Perdew-Burke-Ernzerhof (PBE) functional in density-functional theory (DFT) calculations, Cs*X* materials do not adopt their namesake structure. Furthermore, peculiar low thermal conductivities have been observed experimentally in both CsCl and CsI at room temperature, and the origin has been linked to low-temperature anharmonicity derived from different types of experiments. In the case of CsCl the anharmonicity was observed from x-ray diffraction as an octahedral nuclear probability density function (nPDF), which, in contrast to expectations, becomes spherical at elevated temperature. Here, we study the nPDF of CsBr and CsI from single-crystal x-ray diffraction to compare with the findings of CsCl. It is shown that the aspherical features become less pronounced when substituting for a heavier halide. From periodic DFT calculations on CsCl, CsBr, and CsI probing the potential-energy surfaces this can be explained by progressively more similar masses upon substitution linked with Pauli repulsion. The apparent disappearance of the anharmonic features in CsCl with increasing temperatures can be understood as relatively larger population of acoustic phonons compared to the optical phonons following the Bose-Einstein distribution function. Finally, it is shown that theory can reproduce the correct equilibrium structures as well as phonon dispersions comparable to experimental values when adding a functional form of van der Waals interactions to a PBE DFT calculation.

DOI: 10.1103/PhysRevB.105.104113

I. INTRODUCTION

The cesium halides (Cs*X*), with the exception of CsF, crystallize in the simple highly symmetric "cesium chloride" crystal structure. The chemical interactions are expected to be highly ionic as the structure is formed between a cation with very low electronegativity, and anions with very high electronegativity. The archetypical cesium chloride structure is typically observed for large cations that are similar in size to the anion. This near-perfect, rigid high-symmetry crystal structure is expected to have limited phonon scattering, and correspondingly Cs*X* materials should have a high thermal conductivity, κ. Curiously, very low thermal conductivities of 1.0 and 1.1 W m^{-1} K^{-1} have been observed in CsCl and CsI at room temperature, whereas high κ's were observed at low temperature [1,2]. Low thermal conductivity is often linked to anharmonic vibrations or structural defects [3], but neither of these are expected to be significant in the cesium halides. Surprisingly, significant fourth-order anharmonicity was observed at 20 K in CsCl from analysis of x-ray diffraction data using the Gram-Charlier expansion of the harmonic Debye-Waller factor [1,4]. This refined nuclear probability density function (nPDF) at 20 K had an octahedral shape with lobes pointing towards each face center, but with increasing temperatures the nPDF became progressively more spherical. This apparent disappearance of anharmonicity at elevated temperature is counterintuitive to the common assumption of anharmonicity originating from the progressively larger displacement in a nonparabolic potential and correspondingly larger emphasis on the high-order terms of the potential-energy surface at elevated temperatures.

In the case of CsI, the origin of the low room temperature κ was studied by inelastic neutron scattering and theoretical phonon calculations using density-functional theory (DFT) [2,5,6]. It was found that the trend in κ with temperature could be accounted for with anharmonic low-temperature acoustic phonon modes undergoing three-phonon Umklapp scattering [7,8] of the type (a, a, a) absorption and (a, a, o) emission (a: acoustic, o: optical). The mechanism was generalized to the remaining Cs*X* structures, excluding CsF which adopts the rocksalt structure at thermodynamic equilibrium.

The two mentioned studies of anharmonicity in cesium halides utilized different methods (x-ray diffraction versus inelastic neutron scattering/DFT) and they studied different systems (CsCl versus CsI). The question arises whether the different methods are probing the same physical phenomenon. The DFT calculations on CsI predict the correct trend in κ when including the three-phonon mode scattering mechanism. On the other hand the x-ray diffraction experiment on CsCl indirectly suggests an increase in κ with increasing T at variance with the observed thermal conductivity [1]. However, it must be stressed that the modeling of the Debye-Waller factor only probes the presence of anharmonic motion, and it is not a measure of κ. It is clearly of interest to investigate whether CsBr and CsI show the same octahedrally shaped

*davide.ceresoli@cnr.it
†bo@chem.au.dk

nPDF as CsCl. It is worth mentioning that anharmonicity is often described qualitatively, but new approaches to quantify anharmonicity are being developed [9].

It has previously been noted by Zhang *et al.* [10] that the common DFT functional Perdew-Burke-Ernzerhof (PBE) [11,12], and even the solid-state optimized PBEsol [13], wrongly predicts CsCl to adopt the rocksalt structure unless dispersion effects are included. In other words, CsCl studied with PBE does not adopt its namesake structure type without dispersion corrections. The strength of van der Waals interactions scales with the number of electrons and cesium with 55 electrons and a large static polarizability could exhibit significant van der Waals interactions compared to the remaining alkali halides. Even so, the ionic interactions would be expected to be dominant when the electronegativity difference is as large as 2.2 on the Pauling scale and van der Waals interactions would be a relatively small but significant contribution arising from instantaneous temporary Cs-Cs dipole formation interactions. Ionic interactions generally favor dense structures and in this case the van der Waals interactions' relatively small contribution seem to stabilize the CsCl structure compared to NaCl. Zhang *et al.* obtained the correct cesium chloride structure when adding Grimme's D2 parametric dispersion [14] correction to PBE calculations on CsCl, CsBr, and CsI. However, the D2 correction is not a functional of the electron density, but rather an energetic addition to the total energy based on the atomic arrangement, and it acts as a penalty function for "wrong" geometries. It will therefore only affect the electron density indirectly in structure optimization. This can be important when considering phonon calculations as these are derived from the change in energy when perturbing the structure from equilibrium. This change in energy is not necessarily captured from a penalty function description, and it might be necessary to use more advanced van der Waals descriptions such as the nonlocal rVV10 functional [15,16] add-on to common functionals, which act directly on the electron density. Other studies have shown that these kinds of nonlocal functionals improve the accuracy of computations made on ionic solids such as the rocksalt alkali halides [17–19].

Since CsCl has revealed peculiar features in the nPDF, which differ from expectations from the study of low-temperature anharmonicity in CsI, we have chosen to pursue single-crystal synchrotron x-ray diffraction experiments on CsBr and CsI in order to model the thermal motion and compare with CsCl. In addition, calculated phonon dispersions can help elucidate whether the anharmonicities observed from x-ray diffraction and inelastic neutron scattering are connected. Finally, to probe the importance of van der Waals interactions for these kinds of systems, we have tested equilibrium structure predictions as well as phonon dispersions for a selection of functionals.

II. EXPERIMENT

A. Single-crystal x-ray diffraction

X-ray diffraction data were collected on spherical approximately 15-μm-radii single crystals of CsBr and CsI at BL02B1 beamline at SPring8. Diffraction data were measured using an image plate detector, an x-ray wavelength of 0.2478 Å (50 keV), and a temperature of 20 K. Separate frames of 15.5° $\Delta\omega$ and 360 s exposure time were recorded for a full 75.5° ω scan with 0.5° overlap between subsequent frames. The present experimental conditions yield the following benefits: (1) The high x-ray intensity of the synchrotron beam allows measurements on minute crystals, thereby reducing systematic errors related to absorption and extinction. (2) The short x-ray wavelength of the synchrotron beam leads to high resolution in reciprocal space, which in turn facilitates modeling of anharmonic features [4].

The data were indexed, integrated, scaled, and empirically corrected for absorption [20] using the Rigaku Rapid IP-QuarterChi software. In the indexing process, peaks were rejected if $I < 10\sigma(I)$. The integrated intensities were merged using SORTAV [21] and the resulting estimated standard deviations (esd's) were used as standard uncertainties in structural refinements using the independent atom model (IAM). The structures were solved using the Patterson method in SHELXS and refined using SHELXL [22]. A correction for anomalous dispersion at the experimental wavelength was taken from FPRIME [23]. The atomic positions were fixed at the 1*a* and 1*b* Wyckoff positions of space group $Pm\bar{3}m$. An overview of structural and statistical parameters from the refinements is given in Table I.

The $h+k+l$ odd reflections corresponding to body-centered systematic absences ($Im\bar{3}m$ symmetry) present a particular challenge for cesium halides, and especially for CsI. Cs^+ and I^- are isoelectronic, and therefore the destructive interferences observed in these reflections are almost complete. Close inspection of the frames shows weak low-order reflection (see Fig. 1), but at high angle the odd reflections become essentially indistinguishable from the background. Practically, these peaks are close to the noise level, which means that roughly 50% of reflections are "missing" relative to the expected diffraction pattern of the known symmetry $Pm\bar{3}m$. In the case of CsBr, the odd peaks are clearly visible and inclusion of the peaks in the refinements was straightforward. Inclusion of the odd reflections in the integration of the CsI frames contaminated the extracted value of the even reflections, resulting in poor statistical parameters for the final models. However, completely ignoring the odd reflections led to physically doubtful atomic displacement parameters (ADPs). The solution was to merge a body-centered integrated structure factor list with the odd reflections of a primitive integrated structure factor list by scaling the mean of the even reflections in between the lists; the details of this is included in the Supplemental Material (S1 and S3) [24]. The absence of reflections in compounds of isoelectronic ions is by no means a new observation, but dates back to the early days of x-ray crystallography where KCl showed a diffraction pattern as if both constituent atoms appeared with monovalent charges [25].

Furthermore, for CsI two of the low-order reflections ($(\bar{1}10)$, $(10\bar{1})$) were overexposed and also removed; see Supplemental Material (S1). In the case of electron density modeling this could be detrimental as the information of the diffuse valence electron distribution is located in the low-order reflections [26]. However, for analysis of the thermal motion, which manifests itself as damping of the high-order reflections

TABLE I. Experimental conditions and corrections, unit cell parameters, and statistical and refined parameters in a joint multipolar and Gram-Charlier anharmonic refinement. *X* denotes the corresponding halide.

	CsBr	CsI
T (K)	20	20
r_{sphere} (μm)	∼15	∼15
λ (Å)	0.247 8	0.247 8
$\sin\theta/\lambda$ (Å^{-1})	1.666 7	1.666 7
$T_{\text{max}}/T_{\text{min}}$	1.412 2	1.642 3
Cs: f'/f'' [a]	−0.267 65/2.031 01	−0.267 65/2.031 01
X: f'/f'' [a]	−0.158 84/0.372 18	−0.103 74/1.780 41
μ (mm^{-1})[a]	4.369	5.778
N_{measured}	3975	2100
N_{unique}	352	208
Completeness	1.000	0.501[b]
Average redundancy	11.3	10.1
R_{merge} (%)	3.65	6.12
Space group	$Pm\bar{3}m$	$Pm\bar{3}m$[c]
a (Å)	4.2501(5)	4.5153(5)
V (Å)	76.772(15)	92.055(18)
Z	1	1
min($\sin\theta/\lambda$) (Å^{-1})	0.000 0	0.180 0
max($\sin\theta/\lambda$) (Å^{-1})	1.666 7	1.666 7
$N(I > 3\sigma)$	351	217[d]
$N_{\text{ref}}/N_{\text{var}}$	43.9	31.00
$R(F)$ (%)	1.53	2.45
$R(F^2)$(%)	2.16	4.22
GoF$_w$	1.20	1.50
$\Delta\rho_{\text{min}}$	−1.39	−2.25
$\Delta\rho_{\text{max}}$	2.12	2.28
Extinction	N/a	N/a
Max extinction (%)	N/a	N/a
U_{iso}(Cs) (Å^2)	0.004 43(7)	0.006 0(2)
U_{iso}(X) (Å^2)	0.004 49(4)	0.005 7(1)
δ^{1111}(Cs) · 10^4	0.000 37(7)	0.001 5(3)
δ^{1122}(Cs) · 10^4	0.000 11(3)	0.000 5(1)
d_{00}(Cs) (#e)	0.020(9)	0.020 8
d_{40}(Cs) (#e)	0.006(17)	0.03(2)
d_{44+}(Cs) (#e)	0.005(13)	0.02(1)
d_{00}(X) (#e)	0.147(9)	0.145 6
d_{40}(X) (#e)	0.000 2(28)	0.000 3(55)
d_{44+}(X) (#e)	0.000 1(20)	0.000 2(41)

[a]Calculated with FPRIME [23].
[b]Corresponds to a completeness of 1.000 when merging in the space group $Im\bar{3}m$.
[c]Symmetry used after integration. $Im\bar{3}m$ was only used to integrate reflections initially.
[d]Ten reflections are added from the $Pm\bar{3}m$ integration and the overexposed low-order reflection is removed.

[4], the removal of two low-order reflections has negligible influence on the refinements.

B. Multipolar electronic and anharmonic motion modeling

The structural parameters from the IAM refinement were imported into XD2016 [27]. Scattering factors were taken

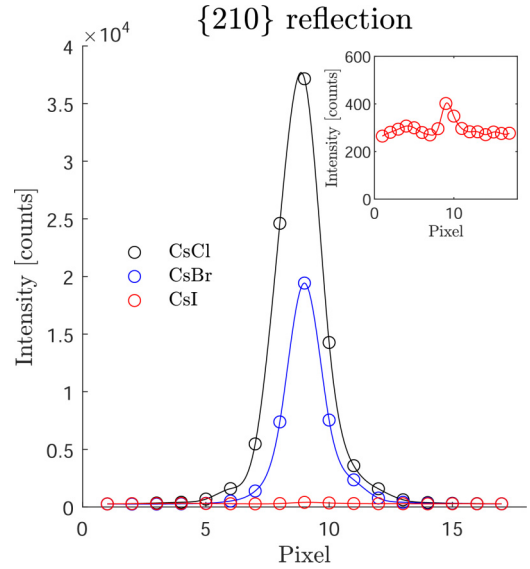

FIG. 1. Intensity count in pixels across maxima of reflections belonging to the family {210} in CsCl, CsBr, and CsI. In the case of CsCl, we are using the same data as Sist *et al.* [1] in order to plot the relative peak intensity. The average of the first and last pixel is equalized between the datasets, bringing them on a common scale. The plot clearly shows a decrease in peak intensity from substituting for a heavier halide and the peak becomes close to indistinguishable from the background in the CsI dataset. The inset shows the peak in the CsI dataset on a different scale—there is a peak but it is close to the background.

from the Volkov-Macchi databank included in XD based on relativistic PBE calculations, and anomalous dispersion was corrected with FPRIME. The esd's were used as weights, and all refinements were made against F^2.

The modeling of anharmonic motion is most often and successfully modeled in the statistical Gram-Charlier (GC) formalism [4,28,29]. Here, the trivariant normal distribution [in this case the anisotropic probability density function $P_0(\mathbf{u})$] is differential series expanded to give a sum of Hermite polynomials, $H_{j\ldots n}(\mathbf{u})$, and quasimoments, $c^{j\ldots n}$,

$$P(\mathbf{u}) = \left[1 + \frac{1}{3!}\gamma^{jkl}H_{jkl}(\mathbf{u}) + \frac{1}{4!}\delta^{jklm}H_{jklm}(\mathbf{u}) + \ldots\right]P_0(\mathbf{u}). \tag{1}$$

The associated Debye-Waller factor is given by the analytic expression via Fourier transformation:

$$T(\mathbf{H}) = \left[1 - \frac{4}{3}\pi^3 i\gamma^{jkl}h_j h_k h_l + \frac{2}{3}\pi^4\delta^{jklm}h_j h_k h_l h_m + \ldots\right] \times T_0(\mathbf{H}), \tag{2}$$

where h_j is the jth Miller index of the reciprocal lattice vector $\mathbf{H}$. The resulting structure factor incorporating anharmonic motion is then given by

$$F(\mathbf{H}) = \sum_j f_j \exp(2\pi i\mathbf{H}\cdot\mathbf{r}_j)T_j(\mathbf{H}). \tag{3}$$

The scattering factor f_j can be chosen as the free spherical atomic scattering factors. A better description accounting

for valence density deformation would be aspherical scattering factors following, e.g., the Hansen-Coppens multipole formalism [30].

It is worth mentioning that the Gram-Charlier formalism in itself does not carry any *a priori* known temperature dependence [28,31]. A temperature dependence can be found for the Gram-Charlier parameters under the assumptions of the classical limit (high-temperature) and independent oscillators (Einstein oscillator) by equating parameters of like **H** dependence between the mathematical Gram-Charlier expansion to the one-particle potential model [4,28]. However, the following experiment is performed at 20 K, which can hardly be called high temperature and it neglects that the atomic oscillators are coupled.

The possible presence of thermal diffuse scattering (TDS), which peaks underneath the Bragg peaks, will increase the observed dampening in reciprocal space, consequently increasing the refined ADPs [29,32]. Furthermore, the anisotropy in the TDS around a Bragg peak has been shown elsewhere in a powder diffraction experiment to affect the refined parameters, e.g., site occupancies [33]. Neither of these effects are assumed to be detrimental for the Gram-Charlier analysis. Individual peaks are integrated, circumventing to an extent the effect of an anisotropic distribution of TDS around the peaks when performing azimuthal integration in powder experiments, and the TDS is assumed isotropically distributed for symmetry-equivalent reflections only affecting the spherical ADP by increasing the dampening in reciprocal space.

Because of the cubic $m\bar{3}m$ symmetry of the occupied Wyckoff positions, only a few degrees of freedom are available. The positions are fixed, and the Gram-Charlier parameters up to, and including, fourth order have the following constraints: $U^{11} = U^{22} = U^{33}$, $\delta^{1111} = \delta^{2222} = \delta^{3333}$, $\delta^{1122} = \delta^{2233} = \delta^{1133}$, while all other GC parameters are zero. Here, U^{jk} is the anisotropic ADPs and δ^{jklm} are the fourth-order quasimoments. Furthermore, the cubic site symmetry mixes the spherical harmonics used to model the valence electrons and therefore it is necessary to employ density normalized Kubic harmonic functions [25,34,35]. For the given site symmetries up to, and including, hexadecapoles, only K_0 and K_4 are available, the former being a monopole and the latter is expressed in terms of the density normalized spherical harmonics, d_{lmp}:

$$K_4 = 0.782\,45 d_{40} + 0.579\,39 d_{44+}. \tag{4}$$

A multitude of models has been tested and they are presented in the Supplemental Material (S2 and S3) [24] while the final models are listed in Table I. The overall refinement strategy of the final models has been to perform high-order (only include $\sin\theta/\lambda > 0.800$ Å^{-1}) thermal motion refinement using the GC formalism. This is followed by locking the thermal parameters and refining the Kubic harmonics in the multipole electron density model and then finally a total refinement—both against the entire resolution range. Thermal motion and aspherical density parameters are correlated and this strategy decouples them by basing the thermal parameters on a section of reciprocal space where valence electron features do not contribute—a consequence of the properties of Fourier transformation. Extinction [36,37] was tested on these models, however proved to be insignificant, nonconvergent, or worsening the fit. Finally, to compare with the model refined by Sist *et al.* [1], an anharmonic-only model has been refined for both systems with an upper limit on resolution of 1.250 Å^{-1} (S5) [24].

C. Theoretical calculations

The crystal structure of the CsX in $Pm\bar{3}m$ has been optimized using the projector augmented-wave (PAW) method [38] as implemented in QUANTUM ESPRESSO within DFT. PBE+rVV10 [15,16] has been used as the exchange-correlation functional. Pseudopotentials [39] for PAW calculations including scalar relativistic effect were used. The cation pseudopotentials included semicore states, i.e., the neutral atom valence state of the cation and anion were $(n-1)s^2(n-1)p^6ns^1$ and ns^2np^5, respectively. A plane-wave energy cutoff of 100 Ry and density energy cutoff of 800 Ry was used in all cases. Reciprocal space was sampled using a k grid of size $12 \times 12 \times 12$ for CsF and $8 \times 8 \times 8$ for the remaining CsX. CsF is included artificially in the cesium chloride structure for comparison.

Phonon dispersions have been calculated within linear response/density-functional perturbation theory on $6 \times 6 \times 6$ (CsF) and $4 \times 4 \times 4$ (remaining CsX) k grids. Born effective charges were calculated to account for the change of dipole moment for optical modes and consequently the splitting of transverse and longitudinal optical branches. A simple acoustic sum rule [40] is applied to the dynamical matrix to ensure that the Γ-point acoustic modes corresponds to translation of the crystal.

Single-point calculations moving along the optical longitudinal Γ-point phonon mode (the stiffest phonon mode) have been calculated using the mass-adjusted eigenvectors of the mode along the ⟨100⟩, ⟨110⟩, and ⟨111⟩ directions to probe the potential-energy surface of this vibration. At 20 K the thermal energy is 1.7 meV, so any mode with this energy will on average contribute with ∼0.5 bosons, while quickly dropping off at higher energy following the Bose-Einstein distribution. Therefore, high-energy phonons contribute to the vibrational free energy only with their zero-point motion. Consequently, it is only a restricted range of the phonon dispersion, which contributes significantly different from zero-point vibration at low temperature to the overall movement of the atoms. Assuming all modes above the thermal energy are equally populated, the stiffest phonon mode potential will give a picture of the potential that mostly restricts the vibration of the system and consequently aspherical features in the nPDF. Note that this potential is not the most significant to determine the overall nPDF; the contribution to the atomic displacement is inversely proportional to the vibrational frequency and thus low-energy phonons are overall more significant when ignoring mode population. However, the Γ-point and Brillouin-zone boundary optical phonons will show similar features but to different extent. Focusing on optical phonons, in the Γ-point mode both atoms vibrate out of phase with each other, while at the Brillouin-zone boundary the heaviest atom is stationary and the lightest atom vibrates. This necessitates a smaller decrease in atomic distances for a given halide displacement and hence a softer potential. The optical phonon at the Γ point will then show the largest deviation

from sphericity if the asphericity is associated with Pauli repulsion between the ions. Multiple modes will show the same asphericity but to a lesser extent until disappearing for significantly small decreases in interatomic distances. We therefore choose to focus on the Γ-point optical phonon mode.

In the case of CsCl and CsI, the structures additionally have been optimized in both the cesium chloride and the rock salt structure using the local density approximation (LDA) [41], PBE, and PBE+rVV10, and specifically for CsCl also PBE+D2. From the equilibrium cesium chloride structures the phonon dispersions were calculated to see to which extent the functionals predict the phonon dispersion obtained from inelastic neutron scattering [2,42].

III. RESULTS

A. Nuclear probability density function

The final models on CsBr and CsI are given in Table I and a series of models are included in the Supplemental Material. Fractal dimension plots and residual density maps are also included in S2-4 in particular S2.4, S3.6, and S4 for the final models. Overall, residual density analysis as formulated by Meindl and Henn [43] clearly shows that Gram-Charlier parameters are necessary in both compounds to describe otherwise systematic residuals. This is independent of whether Kubic harmonic electron density functions are refined or not. Notice that because of the poorly described odd reflections in CsI, the monopole electron density parameters have not been refinable to meaningful values. Furthermore, the Gram-Charlier parameters in a purely anharmonic thermal motion refinement at full resolution and high order, and a coupled anharmonic and aspherical refinement at full resolution yield similar parameters. Especially, the models at full resolution do not show deviations in the Gram-Charlier parameters consistent with the small valence electron population compared with the core electron population. Finally, the fractal dimension plots from only modeling thermal motion at a restricted resolution of 1.25 $Å^{-1}$ also indicate the necessity of fourth-order Gram-Charlier parameters as the statistical significance of the GC parameters decreases making one of them insignificant (S5) [24].

In the article by Sist *et al.* [1] an anharmonic significance factor was defined. This related the size of the anharmonic parameter δ^{1111} to the size of the harmonic parameter $U_{\text{iso}} = U^{11}$, and it is observed that the significance factor decreases with increasing temperature. From their supporting information it seems that the decrease in anharmonicity is in large part due to an increase in second-order parameters. Consequently, there is an increasing spherical contribution to the nPDF as the temperature is increased. But, assuming the second-order contribution to the nPDF at 20 K is sufficiently small to show aspherical features and similar in CsBr and CsI, the asphericity of the nPDF is related to the unitless factor:

$$\alpha = \delta^{1111}/\delta^{1122}. \tag{5}$$

Bear in mind that the turning point from octahedral to cube is not necessarily at $\alpha = 1$. The possible aspherical features can then be drowned out by the second-order contribution. In the order CsCl, CsBr, and CsI, the value of α decreases (4.64 → 3.36 → 3.00). This decrease in α is mirrored in the nPDF as seen in Fig. 2 where only CsCl shows asphericity on a natural log scale while the remaining compounds are spherical. Fairly large fourth-order GC parameters for CsI are refined and they are likewise mirrored in the nPDF showing quite flat nPDF around the outermost contour levels. These might be linked to flat potentials allowing the ion to rattle

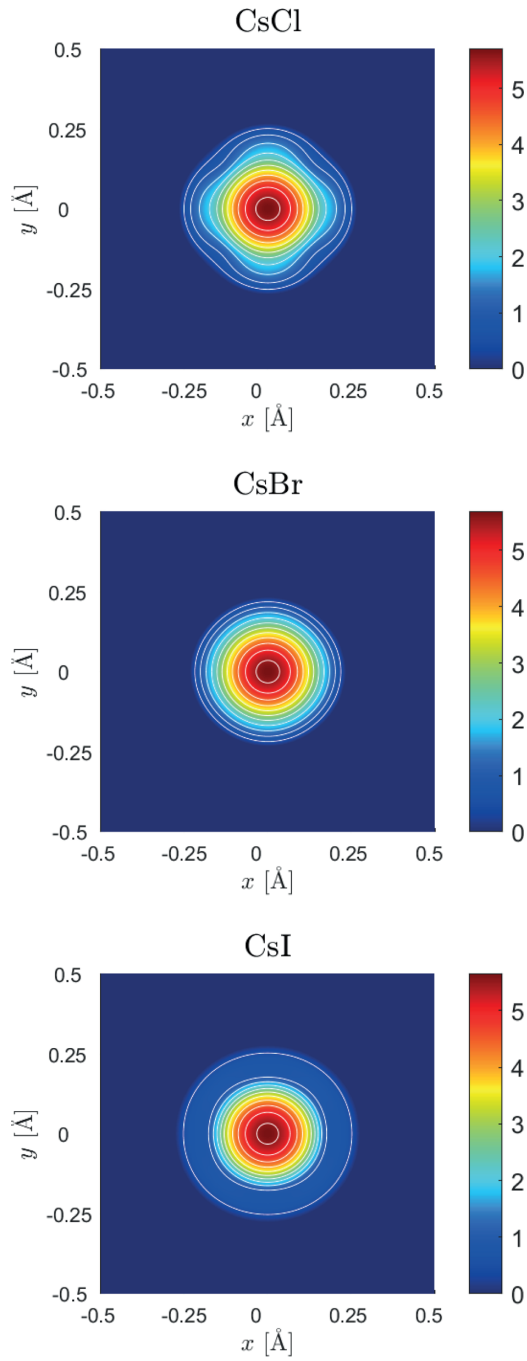

FIG. 2. nPDF of Cs in the anharmonic models of CsCl, CsBr, and CsI at 20 K. The CsCl nPDF is generated from the model parameters of Sist *et al.* [1] The CsBr and CsI nPDFs are generated from the full-resolution model. The probability is plotted on a natural logarithmic color scale. Contour lines are superimposed on the image as white lines. x and y are the distance from the equilibrium position of Cs along the directions ⟨100⟩ in units of angstrom.

within the system or it is an artifact of uncertainty in the dataset.

B. Geometry optimization and phonon dispersions

The energy per formula unit at optimized geometry is included in Supplemental Material (S6) for CsCl and CsI using different functionals in the rocksalt and cesium chloride structure. In both cases, PBE predicts the rocksalt structure, while the remaining functionals correctly predict the cesium chloride structure. From the observations of Zhang *et al.* [10], the failure of predicting the correct equilibrium structure appears to be generalizable to other generalized gradient approximation (GGA) functionals, including PBEsol. Comparing with the experimental unit-cell parameter, a, at 20 K shows that LDA underestimates a, PBE overestimates a, and PBE+rVV10 and PBE-D2 outperform both LDA and PBE and equally deviate from the experimental value. This is the trend observed, e.g., for noble gas adsorption to metal surfaces [44] and graphene interlayer interactions [45], both mainly governed by van der Waals interactions, where LDA overbinds and PBE does not bind at all. From the equilibrium structure calculations, it appears that van der Waals interactions are important for both CsCl and CsI.

In Fig. 3 theoretical phonon dispersion curves are shown together with experimental inelastic neutron scattering values measured by Ahmad *et al.* [42] and Wei *et al.* [2]. For CsCl, PBE-D2 completely fails at predicting the absolute phonon branches, even though it gives a unit-cell estimate of equal quality to PBE+rVV10. The LDA, PBE, and PBE+rVV10 calculations show similar features in the phonon dispersions, but the absolute values of the LDA branches do not correspond well with the experimental values. PBE compares better with experiment, and PBE+rVV10 is clearly the best calculation of the phonon dispersion. The LDA branches shows discrepancies with the experimental values no matter whether finite displacement from phonopy or linear response in QUANTUM ESPRESSO is used. When using VASP with the same computational parameters as in the study by Wei *et al.* [2] their reported phonon branches are correctly reproduced and fit the experimental values. Even though the pseudopotentials are generated by the same method in VASP and QUANTUM ESPRESSO the final calculations appear to differ. The present conclusion is that calculations in QUANTUM ESPRESSO give a better agreement with phonon observations with more complex functionals.

Interestingly, the phonon dispersions clearly show that the dispersion correction by Grimme works well at predicting structure, but it is poor at calculating phonons. In essence, Grimme's correction acts as a penalty function for wrong atomic configurations. The penalty for a wrong configuration does not accurately represent the potential that the atoms are moving in. However, when introducing van der Waals interactions through rVV10, it is possible to obtain a good agreement with inelastic neutron scattering results and predict the correct structure. rVV10 is in fact the only of the tested functionals which predicts the correct structure, and simultaneously is in agreement with the experimental unit cells and phonon

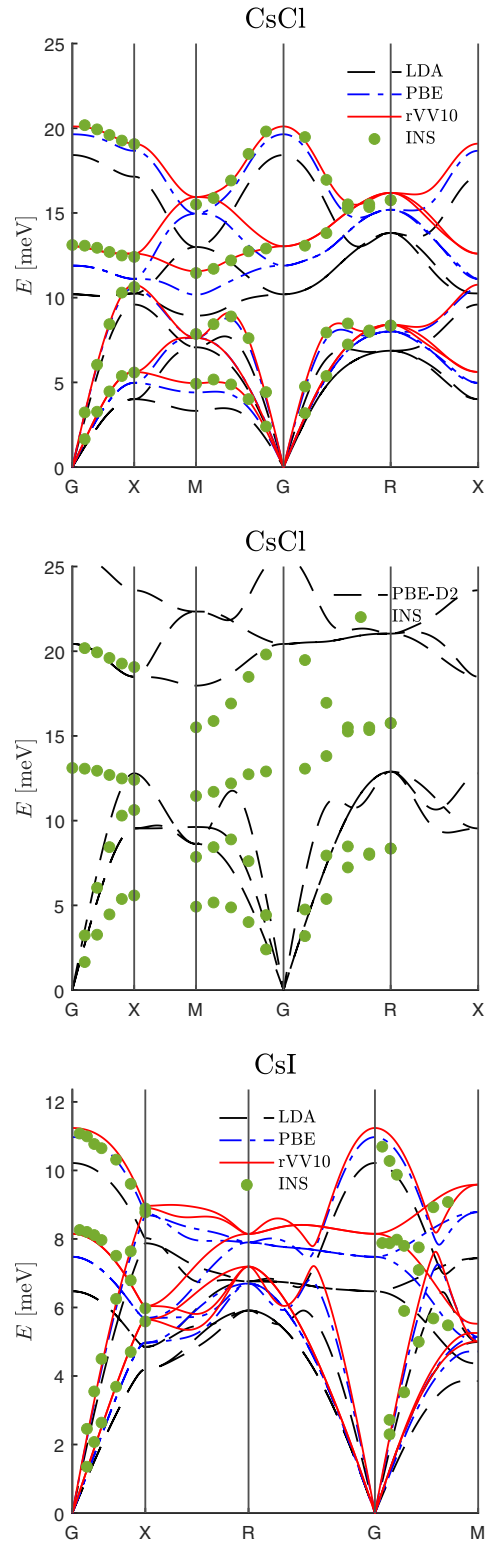

FIG. 3. Phonon dispersions for CsCl and CsI. The data points are determined from inelastic neutron scattering by Ahmad *et al* (CsCl) and Wei *et al* (CsI) [2,42]. The dispersions are calculated using the optimized structure from PBE+rVV10. In the case of CsI LDA, the LDA optimized structure was also tested, but it had no effect on the final dispersion curves.

dispersions. Overall, van der Waals interactions indeed seem to be important for the Cs*X* as stated by Zhang *et al.* [10], but it is important to include a functional description of van der Waals interactions and not just a parametric correction.

C. Potential of longitudinal optical phonon mode

The longitudinal optical mode extracted from QUANTUM ESPRESSO corresponds to a wave vector, q, for which $q \parallel \langle 100\rangle$ and $|q| \to 0$. Taking the appropriate linear combination to align it along $\langle 100\rangle$, $\langle 110\rangle$, and $\langle 111\rangle$, it is possible to probe the potential that Cs vibrates in by performing stepwise single-point calculations moving both atoms along the phonon mode eigenvectors. The potentials are shown in terms of Cs displacement in Fig. 4 together with the potentials and relative potentials in a reduced mass coordinate system. Notice that the potential of the longitudinal optical and acoustic phonon branch at the Brillouin-zone boundary will be similar to the ones shown in Fig. 4, but with less steep potentials since the distance between the atoms are decreased less for these vibrations compared with the optical longitudinal branch at Γ. This directly implies less difference between the three directions for the progressively softer vibrational modes in the systems and thus progressively less aspherical vibrational motion as q approaches the Brillouin-zone boundary in the optical branch.

The difference between $\langle 111\rangle$ and $\langle 100\rangle$ for a given Cs displacement increases with larger displacements in all cases implying that vibrations along $\langle 111\rangle$ are more restricted compared with $\langle 100\rangle$ in agreement with the larger electron density overlap between anion and cation from the $\langle 111\rangle$ vibration compared with $\langle 100\rangle$. However, for a given Cs displacement the difference between $\langle 111\rangle$ and $\langle 100\rangle$ decreases going from CsF to CsI. This agrees very well with the calculated nPDF where it is octahedral for CsCl, but becomes spherical for CsBr and CsI.

Changing from d_{Cs} with an implied halide displacement to a reduced mass coordinate $\sqrt{\mu}d_{\mathrm{Cs}}$ shows the same trend for a given displacement with the lighter cesium halides having a more restrictive potential along $\langle 111\rangle$ relative to $\langle 100\rangle$ compared to the heavier ones. This can be seen from the bottom row in Fig. 4, where the potentials are plotted against the squared reduced mass coordinate and the relative difference of $\langle 111\rangle$ and $\langle 100\rangle$ are plotted against the reduced mass coordinate.

The differences between the systems are essentially the mass and the polarizability of the halide, both increasing when going down group 17 in the Periodic Table. The polarizability could be linked to the observed potential as an increased polarizability would give a softening of the vibration as the electron cloud can more easily rearrange itself around the nuclei. This would favor a less steep increase in potential energy for the vibration of CsI along $\langle 111\rangle$ compared with CsCl.

Simultaneously, the progressively heavier halides lead to a smaller displacement of X for a given displacement of Cs as the mass becomes comparable to Cs. This results in a smaller overlap between the electron density of the atoms, so Pauli repulsion is not introduced before the atoms are displaced significantly more than observed experimentally at low temperature. This would decrease the relative importance of the quartic term to the potential and would result in a spherical nPDF.

It is puzzling why anharmonicity is not observed for the experimental nPDF of Cl in CsCl even though it should have larger displacements. This might be linked to the relatively smaller scattering factor of Cl compared to Cs, which makes the scattering from Cs drown out anharmonic contributions from Cl. With the lower scattering factor, the accompanied x-ray diffraction contribution might not be large enough to be visible in the diffraction peaks intensity for the experimental setup.

D. Asphericity and anharmonicity

The longitudinal optical phonon at Γ fits with the observed nPDF of CsCl, CsBr, and CsI, where the aspherical nPDF disappears for the heavier cesium halides. However, this mode and the similar optical modes at lower energy will not be significantly excited at 20 K. This follows directly from the Bose-Einstein distribution. The optical phonons can nevertheless still explain the observed nPDF and be unified with the measured thermal conductivity. From a diffraction experiment, the harmonic atomic displacement

$$U^{jk} = \langle u^{jk}\rangle \tag{6}$$

can be expressed in terms of the phonon dispersion as

$$\mathbf{U}(\kappa) = \frac{1}{Nm_\kappa}\sum_{i\mathbf{q}}\frac{E_i(\mathbf{q})}{\omega_i^2(\mathbf{q})}\mathbf{e}(\kappa|j\mathbf{q})\mathbf{e}^{*\mathrm{T}}(\kappa|j\mathbf{q}), \tag{7}$$

with κ denoting an atom in the unit cell, i the phonon branch, $\mathbf{q}$ the wave vector, $\mathbf{e}$ the polarization vector, N the number of unit cells, and m_κ the mass of the κth atom [29]. The energy, E_i, of a quantum harmonic oscillator entering the expression is

$$E = \hbar\omega\left(\tfrac{1}{2} + n_{\mathrm{BE}}\right), \tag{8}$$

with n_{BE} being the Bose-Einstein distribution. Within this simple picture, the high-energy phonons will essentially only contribute with their zero-point vibration with a scaling of ω^{-1}. Simultaneously, the phonons with energy up to the thermal energy at 20 K essentially correspond to long-wavelength acoustic modes that do not change appreciably the distance between first neighboring atoms. Following from this, most modes contributing to the matrix $\mathbf{U}$ are approximately populated by 0 phonons, and the shape of the nPDF is then governed by an ω_i^{-1}-weighted sum of zero-point vibrating phonon modes.

The low-energy phonon modes will approximately yield a spherical nPDF while the high-energy phonon modes yield an octahedrally shaped nPDF. The aspherical appearance of the nPDF in CsCl and the disappearance of the asphericity can then be explained by relative populations: At low temperature, essentially only zero-point vibration is present, and the combined nPDF is a weighted average of the vibrational modes giving an aspherical nPDF. At higher temperatures, the low-energy phonon modes will be populated relatively more than the high-energy phonon modes and consequently the spherical features of the nPDF will be more prominent until the aspherical features are drowned out at sufficiently high

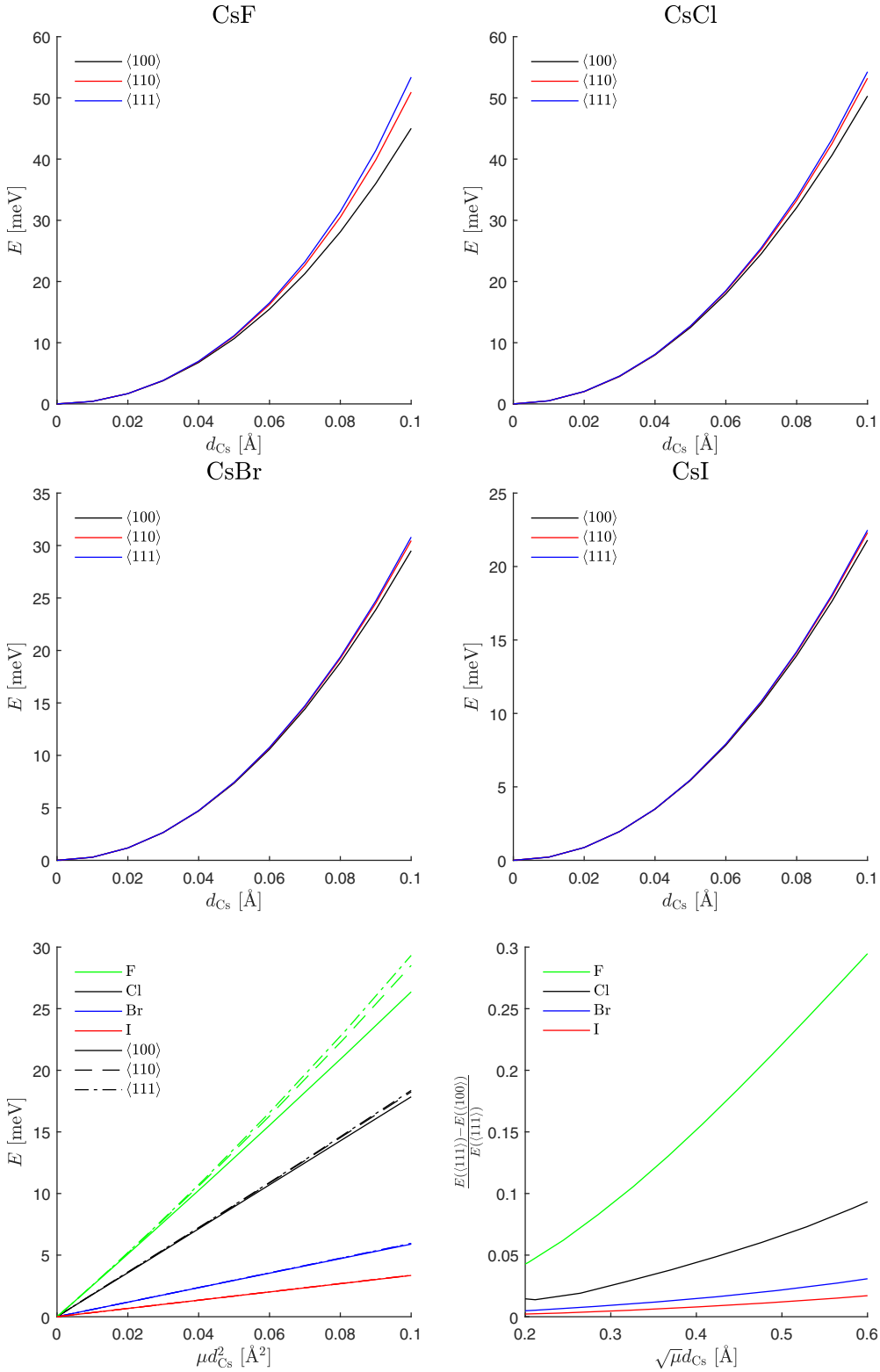

FIG. 4. Confining potential of longitudinal optical phonon at Γ. The x axis maps the displacement of Cs d_{Cs}, but due to the mass difference of cation and anion a given d_{Cs} is accompanied by a displacement of X by $-\sqrt{\frac{m_{Cs}}{m_X}} d_{Cs}$. The lower row shows the potentials plotted against the square reduced mass coordinate to show deviations from harmonicity, and the relative difference between ⟨100⟩ and ⟨111⟩ vs the reduced mass coordinate. Notice that in all cases the steepness of the curves increases as ⟨111⟩ > ⟨110⟩ > ⟨100⟩.

temperatures. This is not observed for CsBr and CsI because at low temperature the nPDF is already spherical.

That the asphericity, and thus the perceived anharmonicity from the optical phonons in CsCl, disappear at elevated temperatures seems, at first, in disagreement with the measured thermal conductivity. However, a decrease in thermal conductivity from phonon-phonon scattering requires n_{BE} to be significantly different from 0 and therefore, at low temperature, where anharmonicity is observed in the nPDF, there are only few phonons available to be scattered. At elevated temperature, the asphericity disappears because of the relatively more populated spherical anharmonic acoustic phonons, but now the populations are large enough to accommodate the scattering mechanisms as presented by Wei *et al.* Consequently, the thermal conductivity decreases even though the nPDF becomes spherical.

The observations that only CsCl has an aspherical nPDF at low temperature [1], which in the current study is interpreted in terms of optical phonons, and that CsCl and CsI have low thermal conductivities associated with anharmonic acoustic phonons [2], are not mutually exclusive. Firstly, both compounds exhibit significant Gram-Charlier parameters and, consequently, both compounds possess low-temperature anharmonicity. Secondly, a proper linear combination of Gram-Charlier parameters can approximate a spherical nPDF and simply visualizing the nPDF alone would lead to the wrong conclusion of absence of anharmonicity as exemplified by CsBr and CsI in the current study. Thirdly, according to the present study, the acoustic phonons would not yield an aspherical nPDF. That is, the anharmonicities observed in the nPDF and the inelastic neutron scattering are different where the latter is associated with thermal conductivity.

IV. CONCLUSION

From x-ray diffraction, it has been possible to show that CsBr and CsI do not exhibit the same octahedrally shaped nPDF as observed for CsCl. This is in agreement with the longitudinal optical potentials, which become progressively more spherical when substituting for a heavier halide. The trend can be explained from relatively stronger potentials in the ⟨111⟩ direction compared with the ⟨100⟩ direction arising from Pauli repulsion linked with the relatively large contribution of zero-point vibration at low temperature. The disappearance of aspherical nPDF for CsCl at elevated temperature can be understood by zero-point vibrations from the optical phonons being drowned out by the relatively more populated acoustic phonons, which have a spherical nPDF.

The present study does not disagree with the microscopic mechanism proposed by Wei *et al.* for the decrease in thermal conductivity of the cesium halides systems with increasing temperature. Rather, it indicates that the anharmonicity observed via the nPDF in CsCl is not linked to the thermal conductivity. Instead, it is linked to the anharmonic optical phonons, which are not populated at low temperature and therefore cannot contribute to thermal conductivity. At high temperature acoustic phonons can combine to yield an optical phonon and decrease the thermal conductivity; however, when the acoustic phonons are sufficiently populated for this mechanism to be active, the optical phonons are already drowned out by the acoustic phonons in the nPDF of CsCl.

It has been shown that a good agreement on phonon dispersions can be achieved between experimental inelastic neutron scattering data and theoretical calculations with both PBE and PBE+rVV10, where the latter in general gives the best agreement. In addition, PBE+rVV10 also predicts the correct structure unlike the PBE functional, which predicts Cs*X* to adopt the rocksalt structure. The simpler approach of adding Grimme's D2 correction to PBE predicts the correct structure, but it significantly overestimates the phonon frequencies. This indicates that van der Waals interactions are important for the Cs*X* systems. Furthermore, it might be relevant to consider van der Waals interactions when performing computations on, e.g., the optoelectronic cesium lead halide perovskites [46].

The significance of anharmonicity does not disappear when substituting for a heavier atom in the Cs*X* family of compounds; however, the difference in energy for the ⟨100⟩, ⟨110⟩, and ⟨111⟩ directions decreases with the heavier halide making the directions indistinguishable from an x-ray diffraction point of view. Consequently, Cs in CsCl has an octahedrally shaped nPDF at low temperature, while in CsBr and CsI the nPDFs do not visibly deviate from a spherical form. However, because of the coupled motion between cation and anion, Cl is expected to show an aspherical nPDF in contrast to experimental observation. That Cl does not experimentally show an aspherical nPDF is likely linked to the small scattering factor of Cl compared to Cs making the contrast between the atoms large. Meanwhile, the nPDF of neither Br nor I is expected to deviate from sphericity as observed.

ACKNOWLEDGMENTS

We would like to acknowledge Jiawei Zhang for computing the phonon dispersion of CsI with VASP for comparative purposes between our result and the one given by Wei *et al.* Likewise, we would like to acknowledge the beam-time crew Venkatesha Hathwar, Mattia Sist, and Hidataka Kasai for measuring the single-crystal x-ray diffraction data, and the beamline scientist at BL02B1 Kunihisa Sugimoto. We thank Carlo Gatti for fruitful discussions. The computational results were obtained at the Centre for Scientific Computing at Aarhus University. This work was supported by the Villum Foundation.

[1] M. Sist, K. F. F. Fischer, H. Kasai, and B. B. Iversen, Low-temperature anharmonicity in cesium chloride (CsCl), Angew. Chemie Int. Ed. **56**, 3625 (2017).

[2] B. Wei, X. Yu, C. Yang, X. Rao, X. Wang, S. Chi, X. Sun, and J. Hong, Low-temperature anharmonicity and the thermal conductivity of cesium iodide, Phys. Rev. B **99**, 184301 (2019).

[3] C. W. Li, J. Hong, A. F. May, D. Bansal, S. Chi, T. Hong, G. Ehlers, and O. Delaire, Orbitally driven giant phonon anharmonicity in SnSe, Nat. Phys. **11**, 1063 (2015).

[4] W. F. Kuhs, Generalized atomic displacements in crystallographic structure analysis, Acta Crystallogr., Sect. A **A48**, 80 (1992).

[5] P. Hohenberg and W. Kohn, Inhomogeneous electron gas, Phys. Rev. **136**, B864 (1964).

[6] W. Kohn and L. J. Sham, Self-consistent equations including exchange and correlation effects, Phys. Rev. **140**, A1133 (1965).

[7] R. Peierls, Zur kinetischen theorie der wärmeleitung in kristallen, Ann. Phys. **395**, 1055 (1929).

[8] A. A. Maznev and O. B. Wright, Demystifying Umklapp vs normal scattering in lattice thermal conductivity, Am. J. Phys. **82**, 1062 (2014).

[9] F. Knoop, T. A. R. Purcell, M. Scheffler, and C. Carbogno, Anharmonicity measure for materials, Phys. Rev. Mater. **4**, 083809 (2020).

[10] F. Zhang, J. D. Gale, B. P. Uberuaga, C. R. Stanek, and N. A. Marks, Importance of dispersion in density functional calculations of cesium chloride and its related halides, Phys. Rev. B: Condens. Matter Mater. Phys. **88**, 054112 (2013).

[11] J. P. Perdew, K. Burke, and M. Ernzerhof, Generalized Gradient Approximation Made Simple, Phys. Rev. Lett. **77**, 3865 (1996).

[12] J. P. Perdew, K. Burke, and M. Ernzerhof, Generalized Gradient Approximation Made Simple [Phys. Rev. Lett. **77**, 3865 (1996)], Phys. Rev. Lett. **78**, 1396(E) (1997).

[13] J. P. Perdew, A. Ruzsinszky, G. I. Csonka, O. A. Vydrov, G. E. Scuseria, L. A. Constantin, X. Zhou, and K. Burke, Restoring the Density-Gradient Expansion for Exchange in Solids and Surfaces, Phys. Rev. Lett. **100**, 136406 (2008).

[14] S. Grimme, Semiempirical GGA-type density functional constructed with a long-range dispersion correction, J. Comput. Chem. **27**, 1787 (2006).

[15] O. A. Vydrov and T. Van Voorhis, Nonlocal van der Waals density functional: The simpler the better, J. Chem. Phys. **133**, 244103 (2010).

[16] R. Sabatini, T. Gorni, and S. de Gironcoli, Nonlocal van der Waals density functional made simple and efficient, Phys. Rev. B: Condens. Matter Mater. Phys. **87**, 041108(R) (2013).

[17] M. L. Marcondes, R. M. Wentzcovitch, and L. V. C. Assali, Importance of van der Waals interaction on structural, vibrational, and thermodynamic properties of NaCl, Solid State Commun. **273**, 11 (2018).

[18] F. Tran, L. Kalantari, B. Traoré, X. Rocquefelte, and P. Blaha, Nonlocal van der Waals functionals for solids: Choosing an appropriate one, Phys. Rev. Mater. **3**, 063602 (2019).

[19] J. Klimeš, D. R. Bowler, and A. Michaelides, van der Waals density functionals applied to solids, Phys. Rev. B: Condens. Matter Mater. Phys. **83**, 195131 (2011).

[20] R. H. Blessing, An empirical correction for absorption anisotropy, Acta Crystallogr., Sect. A **A51**, 33 (1995).

[21] R. H. Blessing, Outlier treatment in data merging, J. Appl. Crystallogr. **30**, 421 (1997).

[22] G. M. Sheldrick, A short history of SHELX, Acta Crystallogr., Sect. A **A64**, 112 (2008).

[23] D. T. Cromer, Calculation of anomalous scattering factors at arbitrary wavelengths, J. Appl. Crystallogr. **16**, 437 (1983).

[24] See Supplemental Material at http://link.aps.org/supplemental/10.1103/PhysRevB.105.104113 for overexposed detector frame, model parameters of tested models and associated fractal dimension plots and scale plots, calculated energy per formula unit using different functionals, and quartic polynomial fits to potential energy surface.

[25] P. Debye, Laue-Interferenzen Und Atombau, Naturwissenschaften **10**, 384 (1922).

[26] P. Coppens, *X-Ray Charge Densities and Chemical Bonding* (Oxford University Press, Oxford, 1997).

[27] A. Volkov, P. Macchi, L. J. Farrugia, C. Gatti, P. R. Mallinson, T. Richter, and T. Koritsanszky, XD2016 - A Computer Program Package for Multipole Refinement, Topological Analysis of Charge Densities and Evaluation of Intermolecular Energies from Experimental or Theoretical Structure Factors (2016), https://www.chem.gla.ac.uk/~louis/xd-home/.

[28] K. N. Trueblood, H. B. Bürgi, H. Burzlaff, J. D. Dunitz, C. M. Gramaccioli, H. H. Schulz, U. Shmueli, and S. C. Abrahams, Atomic displacement parameter nomenclature report of a subcommittee on atomic displacement parameter nomenclature, Acta Crystallogr., Sect. A **A52**, 770 (1996).

[29] B. T. M. Willis and A. W. Pryor, *Thermal Vibrations in Crystallography*, 1st ed. (Cambridge University Press, Cambridge, UK, 1975) .

[30] N. K. Hansen and P. Coppens, Testing aspherical atom refinements on small-molecule data sets, Acta Crystallogr., Sect. A **A34**, 909 (1978).

[31] B. B. Iversen, S. K. Nielsen, and F. K. Larsen, Reciprocal- and direct-space determination of the temperature dependence of thermal vibrations in magnesium: A neutron diffraction study, Philos. Mag. A **72**, 1357 (1995).

[32] N. Wahlberg and A. Ø. Madsen, Implications of x-ray thermal diffuse scattering in integrated Bragg intensities of silicon and cubic boron nitride, J. Appl. Crystallogr. **50**, 1791 (2017).

[33] C. M. Zeuthen, P. S. Thorup, N. Roth, and B. B. Iversen, Reconciling crystallographic and physical property measurements on thermoelectric lead sulfide, J. Am. Chem. Soc. **141**, 8146 (2019).

[34] F. C. Von Der Lage and H. A. Bethe, A method for obtaining electronic eigenfunctions and eigenvalues in solids with an application to sodium, Phys. Rev. **71**, 612 (1947).

[35] Z. Su and P. Coppens, Normalization factors for Kubic harmonic density functions, Acta Crystallogr., Sect. A **A50**, 408 (1994).

[36] P. J. Becker and P. Coppens, Extinction within the limit of validity of the Darwin transfer equations. I. General formalism for primary and secondary extinction and their applications to spherical crystals, Acta Crystallogr., Sect. A **A30**, 129 (1974).

[37] P. J. Becker and P. Coppens, Extinction within the limit of validity of the Darwin transfer equations. II. Refinement of extinction in spherical crystals of SrFz and LiF, Acta Crystallogr., Sect. A **A30**, 148 (1974).

[38] P. E. Blöchl, Projector augmented-wave method, Phys. Rev. B **50**, 17953 (1994).

[39] A. Dal Corso, Pseudopotentials Periodic Table: From H to Pu, Comput. Mater. Sci. **95**, 337 (2014).

[40] A. A. Maradudin, E. W. Montroll, and G. H. Weiss, *Theory of Lattice Dynamics in the Harmonic Approximation*, 2d ed. (Academic Press, New York, 1971).

[41] J. P. Perdew and A. Zunger, Self-interaction correction to density-functional approximations for many-electron systems, Phys. Rev. B **23**, 5048 (1981).

[42] A. A. Z. Ahmad, H. G. Smith, N. Wakabayashi, and M. K. Wilkinson, Lattice dynamics of cesium chloride, Phys. Rev. B **6**, 3956 (1972).

[43] K. Meindl and J. Henn, Foundations of residual-density analysis, Acta Crystallogr., Sect. A **A64**, 404 (2008).

[44] D.-L. Chen, W. A. Al-Saidi, and J. K. Johnson, The role of van der Waals interactions in the adsorption of noble gases on metal surfaces, J. Phys.: Condens. Matter **24**, 424211 (2012).

[45] H. Rydberg, N. Jacobson, P. Hyldgaard, S. I. Simak, B. I. Lundqvist, and D. C. Langreth, Hard numbers on soft matter, Surf. Sci. **532–535**, 606 (2003).

[46] L. Protesescu, S. Yakunin, M. I. Bodnarchuk, F. Krieg, R. Caputo, C. H. Hendon, R. X. Yang, A. Walsh, and M. V. Kovalenko, Nanocrystals of cesium lead halide perovskites ($CsPbX_3$, X = Cl, Br, and I): Novel optoelectronic materials showing bright emission with wide color gamut, Nano Lett. **15**, 3692 (2015).